Capillary condensation and orientational ordering of confined polar fluids

Matthias Gramzow[1] and Sabine H. L. Klapp[1,2,*]
[1]*Stranski–Laboratorium für Physikalische und Theoretische Chemie, Sekretariat C7, Technische Universität Berlin, Straße des 17, Juni 115, D-10623 Berlin, Germany*
[2]*Institut für Theoretische Physik, Sekretariat PN 7-1, Fakultät II für Mathematik und Naturwissenschaften, Technische Universität Berlin, Hardenbergstraße 36, D-10623 Berlin, Germany*
(Received 12 July 2006; published 29 January 2007)

The phase behavior and the orientational structure of polar model fluids confined to slit pores is investigated by means of density functional theory in a modified mean-field approximation. We focus on fluid states and further assume a uniform number density throughout the pore. Our results for spherical dipolar particles with additional van der Waals–like interactions (Stockmayer fluids) reveal complex fluid-fluid phase behavior involving condensation and first- and second-order isotropic-to-ferroelectric phase transitions, where the ferroelectric ordering occurs parallel to the confining walls. The relative importance of these phase transitions depends on two "tuning" parameters, that is the strength of the dipolar interactions (relative to the isotropic attractive ones) between fluid particles, and on the pore width. In particular, in narrow pores the condensation transition seen in bulk Stockmayer fluids is entirely suppressed. For dipolar hard spheres, on the other hand, the impact of confinement consists in a decrease of the isotropic-to-ferroelectric transition temperatures. We also demonstrate that the local orientational structure is inhomogeneous and anisotropic even in globally isotropic systems, in agreement with computer simulation results.

DOI: 10.1103/PhysRevE.75.011605 PACS number(s): 68.03.Fg, 05.70.Np, 68.18.Jk, 68.15.+e

I. INTRODUCTION

Spatial confinement may have significant effects on the phase behavior of a confined fluid compared to its bulk counterpart [1]. Classical examples are the shift of the bulk gas-liquid condensation towards lower pressures (capillary condensation), the corresponding suppression of the vapor-liquid critical point [2–4], shifts of the freezing temperatures [5,6], or capillary nematization in liquid-crystal models [7–11]. Furthermore, in a recent simulation study [12,13] of strongly coupled dipolar fluids (spherical particles with permanent point dipoles) we have shown that presence of confining walls can even promote long-range parallel ordering of the dipole moments.

In the present paper we are rather concerned with the impact of confinement on moderately polar fluids such as chloroform, where the molecules interact with each other both by anisotropic dipolar and by dispersive (van der Waals) interactions. A classical model for such systems is the so-called Stockmayer fluid [14], whose bulk behavior has been intensely studied over the last decade. In particular, it has turned out [15–17] that Stockmayer fluids with appropriate ratios of dipolar and dispersive interactions can exhibit both a vapor-liquid transition and a second fluid-fluid transition yielding a ferroelectric phase with long-range order of the dipole moments. The characteristics of these two fluid-fluid phase transitions in the presence of two parallel confining walls (slit-pore) are the central topic of our investigation. As an example of a "dipole-dominated system" we also consider a confined dipolar hard sphere (DHS) fluid, in which the ordinary gas-liquid transition is absent [18,19].

So far, confined fluids with dipolar interactions have been much less investigated than systems interacting via short-range (e.g., Lennard-Jones) potentials [20]. The most important reason is the computational burden of handling systems with long-range interactions *and* reduced spatial symmetry. It is therefore not surprising that, prior to our own calculations involving confined dipolar soft spheres [12,13], most theoretical and simulation studies of confined dipolar model fluids had focused on specific thermodynamic states [21–24] and on systems in which the dipolar interactions are essentially unimportant [25–27].

In the present work we explore the phase behavior of Stockmayer and DHS fluids using density functional theory in the so-called modified mean-field (MMF) approximation [28–30]. Within this method, the pair correlation function g involved in the interaction part of the free energy is replaced by the Boltzmann factor (contrary to simple mean-field theory, where g is set to one). The same ansatz has been previously employed to study phase properties of bulk dipolar fluids [31,32] and dipolar mixtures [33], and the results suggest that the theory does reproduce main features of the phase behavior such as the appearance of spontaneous polarization and the presence (absence) of ordinary condensation transitions in pure Stockmayer (DHS) fluids. In order to facilitate investigation of the overall phase behavior we further assume that the number density is uniform throughout the pore. This is clearly an idealization in view of stratification, that is the formation of the fluid molecules into layers (strata) parallel to the confining walls. Experimental evidence for this ordering phenomenon is given by the oscillatory force-distance (solvation force) profiles occurring in a variety of simple and complex confined fluids [34], as well as by the appearance of layering transitions, i.e., the stepwise expulsion of molecules from thin liquid films [35]. Stratification has also be observed directly, that is, via oscillatory density profiles, in computer simulations and theoretical studies (for a recent review, see Ref. [20]) of fluids confined to slit-pore geometries. On the other hand, stratification is usually re-

*Electronic address: sabine.klapp@fluids.tu-berlin.de

stricted to those regions in the fluid immediately exposed to the walls [20]. Therefore, the assumption of a uniform density in our theoretical study seems reasonable at least for mesoscopic pore width, and may serve as a useful starting point even for investigations of nanoscopic pores with pore widths of a few particle diameters.

The rest of the paper is organized as follows. In Sec. II we formulate our model and derive the MMF expression for the free energy functional, focusing on fluid phases with isotropic or orientationally ordered character. The resulting functional is a generalization of the corresponding expression for bulk polar systems derived earlier [29,31,32]. Results for the overall phase behavior and the local orientational structure are presented in Secs. III A and III B, respectively. Finally, our conclusions are summarized in Sec. IV.

II. THEORY

A. Model system

Our model fluid consists of spherical particles with diameters σ and embedded point dipole moment of strength μ in the center of the particles. In addition to the dipole-dipole interaction a Lennard-Jones (LJ) interaction between the spheres may be present as well. The resulting pair potential between two particles with coordinates $(1)=(\mathbf{r}_1,\omega_1)$ and $(2)=(\mathbf{r}_2,\omega_2)$ is given as

$$u_{\mathrm{FF}}(12)=\begin{cases}\infty, & r_{12}<\tilde{\sigma}_T,\\ u^{\mathrm{dip}}(\mathbf{r}_{12},\omega_1,\omega_2)+u^{\mathrm{LJ}}(r_{12}), & r_{12}>\tilde{\sigma}_T,\end{cases} \tag{2.1}$$

where $\mathbf{r}_{12}=\mathbf{r}_1-\mathbf{r}_2$ is the connecting vector, $r_{12}=|\mathbf{r}_{12}|$, and $\omega_i=(\theta_i,\phi_i)$ represents the orientation of particle i in a spatially fixed coordinate system. Furthermore,

$$u^{\mathrm{dip}}(\mathbf{r}_{12},\omega_1,\omega_2)=\frac{\mu^2}{r_{12}^3}\hat{\boldsymbol{\mu}}(\omega_1)\cdot\hat{\boldsymbol{\mu}}(\omega_2)-3[\hat{\boldsymbol{\mu}}(\omega_1)\cdot\hat{\mathbf{r}}_{12}][\hat{\boldsymbol{\mu}}(\omega_2)\cdot\hat{\mathbf{r}}_{12}], \tag{2.2}$$

is the dipolar potential where $\hat{\boldsymbol{\mu}}(\omega)$ and $\hat{\mathbf{r}}_{12}$ are unit vectors in the direction of ω and $\mathbf{r}_{12}$, respectively, and

$$u^{\mathrm{LJ}}(r_{12})=4\epsilon_{\mathrm{FF}}\left[\left(\frac{\sigma}{r_{12}}\right)^{12}-\left(\frac{\sigma}{r_{12}}\right)^{6}\right] \tag{2.3}$$

is the LJ potential involving the attraction parameter ϵ_{FF}. Apart from the hard core in Eq. (2.1), which we have introduced for numerical convenience, the present model is a so-called Stockmayer fluid (see, e.g., Ref. [15]). To mimic the fact that, in the true Stockmayer fluid, the average particle separation varies with the thermodynamic parameters considered, we choose a temperature-dependent hard core defined via the Barker-Henderson (BH) formula [36]

$$\tilde{\sigma}_T=\int_0^{\sigma}dr_{12}\exp[-\beta u_{\mathrm{LJ}}(r_{12})], \tag{2.4}$$

where T is the temperature and $\beta=1/k_BT$ with k_B being Boltzmann's constant. In addition to Stockmayer fluids, we consider in the present work also dipolar fluids without any dispersive interactions, i.e., $\epsilon_{\mathrm{FF}}=u_{\mathrm{LJ}}(r_{12})=0$. In this limit, BH formula gives $\tilde{\sigma}_T=\sigma$, and the pair potential (2.1) reduces to that of dipolar hard spheres.

To model the confinement, we consider the dipolar fluid described by Eq. (2.1) to be squeezed between two plane parallel, smooth walls separated by a distance L_z along the z axis of the coordinate system and of infinite extent in the x-y plane. Specifically, we employ the fluid-wall potential

$$u_{\mathrm{FW}}(z)=\begin{cases}\infty, & |z|>(L_z-\tilde{\sigma}_T)/2,\\ -\frac{2\pi}{3}\epsilon_{\mathrm{FW}}\left[\left(\frac{\sigma}{L_z/2+z}\right)^3+\left(\frac{\sigma}{L_z/2-z}\right)^3\right], & |z|<(L_z-\tilde{\sigma}_T)/2.\end{cases} \tag{2.5}$$

The functional form of $u_{\mathrm{FW}}(z)$ is based on the assumption that each wall consists of particles with which the fluid atoms interact via the LJ potential given in Eq. (2.3). Averaging then the LJ interactions over all possible positions of wall atoms (i.e., the subspaces $z\leq -L_z/2$ and $z\geq L_z/2$) and approximating (for numerical reasons) the averaged repulsive part of the LJ potential by a hard core at $|z|=(L_z-\tilde{\sigma}_T)/2$, one obtains the fluid-wall potential given in Eq. (2.5). We note that, due to the effectively hard walls, the space in directions normal to the walls is restricted to $L_z-\tilde{\sigma}_T$ (rather than to L_z).

In the present calculations we set the fluid-wall attraction parameter ϵ_{FW} equal to that characterizing the fluid-fluid interactions, i.e., $\epsilon_{\mathrm{FW}}=\epsilon_{\mathrm{FF}}$. For $\epsilon_{\mathrm{FF}}=0$ we therefore consider DHS between hard walls, whereas the Stockmayer fluid ($\epsilon_{\mathrm{FF}}>0$) is exposed to additional attractive fluid-wall interactions.

B. Density functional theory

In order to analyze the phase behavior of our confined polar fluid we employ density functional theory. The key quantity of this approach is the grand canonical density functional $\Omega[\rho]$,

$$\Omega[\rho] = F^{\mathrm{id}}[\rho] + F^{\mathrm{FF}}[\rho] + \int d\mathbf{r}_1 d\omega_1 [u^{\mathrm{FW}}(z_1) - \mu_{\mathrm{chem}}]\rho(\mathbf{r}_1, \omega_1), \quad (2.6)$$

where $\rho(\mathbf{r}_1, \omega_1)$ is the singlet density, F^{id} is the ideal-gas part of the free energy, F^{FF} is the (fluid-fluid-) interaction part, and the last term in Eq. (2.6) includes the effect of the external (fluid-wall) potential [see Eq. (2.5)] and the chemical potential μ_{chem}. Per definition, Ω becomes minimal for the equilibrium configuration $\rho(\mathbf{r}, \omega)$ corresponding to the set $(\mu_{\mathrm{chem}}, T, \mathcal{V})$ [where $\mathcal{V}=\mathcal{A}(L_z-\tilde{\sigma}_T)$ is the volume defined by the effective wall separation and the area $\mathcal{A}$ parallel to the walls]. Thus, the singlet density fulfills the Euler-Lagrange equation

$$\frac{\delta\Omega}{\delta\rho(\mathbf{r}, \omega)} = 0. \quad (2.7)$$

1. Singlet density

In this work we restrict ourselves to the treatment of fluidlike, but possibly orientationally ordered phases of the dipolar model fluid in the slit pore. We are particularly interested in the occurrence of spontaneous polarization. In principle, investigation of this situation requires us to take into account the formation of domains with differently directed polarization vectors. By forming domains, a real system (of arbitrary shape) avoids the occurrence of depolarizing fields $\mathbf{E}^D$ arising in homogeneously polarized samples from surface charges at their boundaries (see, e.g., Ref. [37]). Explicit expressions for $\mathbf{E}^D$ can be derived for general ellipsoids [37]. Within density functional theory, domain formation could described by a singlet density $\rho(\mathbf{r}, \omega)$ depending on all three spatial coordinates, but using such an ansatz in the actual minimization procedure is a quite challenging task as demonstrated by recent work of Groh and Dietrich [38,39]. For bulk systems, the same authors have shown [40] that one can circumvent the problem by considering *a priori* a needlelike volume (polarized along its long axis), for which $\mathbf{E}^D=0$ and a homogeneous polarization without domains can be assumed (more precisely, it was shown that the needlelike volume corresponds to the same free energy as a volume of arbitrary shape subdivided into domains). The confined geometry considered in the present work can be considered as an ellipsoid with vanishing aspect ratio. For this geometry, $\mathbf{E}^D$ vanishes [37] if the sample is polarized along a direction in the plane spanned by the slab (contrary to the situation of perpendicular polarization). Therefore, the confined fluid with in-plane polarization is comparable to the bulk fluid in the needlelike volume with longitudinal polarization and indeed, it can be shown that the corresponding free energies can be mapped onto each other [31]. Focusing on this type of polarization we can therefore safely neglect domain formation (further evidence for the absence of domains is given by our recent computer simulation results [12,13]). Thus, the only possible spatial dependence of the singlet density is that induced by the pure confinement and concerns the z direction, that is,

$$\rho(\mathbf{r}, \omega) = \rho(z, \omega) = \rho\alpha(z, \omega). \quad (2.8)$$

In Eq. (2.8) $\alpha(\omega)$ is the orientational distribution function, which is normalized to 1, i.e.,

$$\int d\omega \alpha(z, \omega) = 1. \quad (2.9)$$

For isotropic states, $\alpha(\omega)=1/(4\pi)$. Deviations from that constant value indicate the presence of orientational order. To describe an ordering along a direction parallel to the walls (i.e., within the xy plane), we follow Ref. [31] (where oblate bulk samples have been considered) and expand $\alpha(z, \omega)$ in terms of spherical harmonics $\mathcal{Y}_{lm}(\omega)$ [41],

$$\alpha(z, \omega) = \sum_{l=0}^{\infty} \sum_{m=-l}^{l} \alpha_{lm}(z)\mathcal{Y}_{lm}(\omega), \quad (2.10)$$

where the lowest-order coefficient must be a (real) constant in order to fulfill the normalization condition (2.9), i.e., $\alpha_{00}(z)=\alpha_{00}=1/\sqrt{4\pi}$. The higher-order expansion coefficients are, in general, complex quantities, as are the spherical harmonics. Indeed, one has [41] $\mathcal{Y}^*_{lm}(\omega)=\mathcal{Y}_{l\underline{m}}(\omega)$, where $\mathcal{Y}^*$ denotes the complex conjugate and $\underline{m}=-m$. The requirement that the orientational distribution must be real then imposes the condition $\alpha_{l\underline{m}}(z)=(-1)^m\alpha^*_{lm}(z)$. Finally, the expansion coefficients $\alpha_{lm}(z)$, which may be interpreted as (local) orientational order parameters, are related to the full distribution via

$$\alpha_{lm}(z) = \int d\omega \alpha(z, \omega)\mathcal{Y}^*_{lm}(\omega). \quad (2.11)$$

With the above definitions, the appearance of a polarization $\tilde{\mathbf{P}}(z)=\rho\mu\mathbf{P}(z)$, where $\mathbf{P}(z)=\int d\omega\alpha(z, \omega)\hat{\boldsymbol{\mu}}(\omega)$, is indicated by nonzero order parameters with $l=1$. Indeed, reexpressing the Cartesian components of $\hat{\boldsymbol{\mu}}$ in terms of spherical harmonics and using the expansion (2.10) we find for the Cartesian components of $\mathbf{P}(z)$,

$$P_x(z) = \int d\omega\alpha(z, \omega)\sin\theta\cos\phi = -\sqrt{\frac{4\pi}{3}}\frac{\sqrt{2}}{2}\int d\omega\alpha(z, \omega)[\mathcal{Y}_{11}(\omega) + \mathcal{Y}^*_{11}(\omega)] = -\sqrt{\frac{8\pi}{3}}\mathrm{Re}\,\alpha_{11}(z) \quad (2.12)$$

and, similarly,

$$P_y(z) = \int d\omega\alpha(z, \omega)\sin\theta\sin\phi = \sqrt{\frac{8\pi}{3}}\,\mathrm{Im}\,\alpha_{11}(z),$$

$$P_z(z) = \int d\omega\alpha(z, \omega)\cos\theta = \sqrt{\frac{4\pi}{3}}\alpha_{10}(z). \quad (2.13)$$

As argued at the beginning of this paragraph [see text before Eq. (2.8)], the z component of $\tilde{\mathbf{P}}(z)$ should be zero in any equilibrium configuration, and we will later see that this is indeed the case (see Sec. III). Nevertheless, to check the

calculations we keep the coefficient $\alpha_{10}(z)$ as a minimization parameter. In deriving the right-most members of Eqs. (2.12) and (2.13) we have used the orthogonality of the spherical harmonics, $\int d\omega \mathcal{Y}^*_{lm}(\omega)\mathcal{Y}_{l'm'}(\omega)=\delta_{l,l'}\delta_{m,m'}$, and Re and Im denote real and imaginary parts, respectively. Notice that the Cartesian components of $\mathbf{P}(z)$ are not independent. Indeed, due to the normalization of the distribution $\alpha(z,\omega)$ [see Eq. (2.9)], the magnitude of each component is less than or equal to one, and the same holds for the sum of the squared averages, $P_x^2(z)+P_y^2(z)+P_z^2(z)\leq 1$ (equality holds for perfect alignment of the dipoles). Finally, nonzero order parameters with $l=2$ indicate some type of ordering of the dipole axes. A particularly interesting quantity, which can be nonzero already in isotropic (unpolarized) phases, is the order parameter $\alpha_{20}(z)$ describing the axes' orientation relative to the z axis. In Sec. III B, we will present results for the related (normalized) zz component of the local quadrupole tensor

$$Q_{zz}(z) \equiv \int d\omega \alpha(z,\omega)\frac{1}{2}(3\cos^2\theta - 1) = \sqrt{\frac{4\pi}{5}}\alpha_{20}(z). \tag{2.14}$$

$Q_{zz}(z)=1$ indicates perfect ordering of the dipole axes normal to the walls (i.e., $\cos\theta=0$ for all dipoles). On the other hand, $Q_{zz}(z)=-1/2$ if the dipoles point exclusively along directions in the x-y plane (i.e., $\cos\theta=1$).

The higher-order parameters $\alpha_{2\pm1}(z)$ and $\alpha_{2\pm2}(z)$ are related to the tensor components $Q_{xx}(z)$, $Q_{yy}(z)$, $Q_{xy}(z)$, etc., and describe ordering of the dipole axes relative to other than the z direction. We do not further discuss these quantities since we are particularly interested in axes ordering in the isotropic phase where, as we will see in Sec. III B, $\alpha_{20}(z)$ is the only nonvanishing order parameter.

2. Free energy in modified mean-field approximation

We now turn to the various free energy contributions appearing in the definition (2.6) of the grand canonical density functional. Within the present ansatz for the singlet density [see Eq. (2.8)] the ideal part is given by

$$F^{\mathrm{id}} = \mathcal{V}k_BT\rho[\ln(\rho\Lambda^3)-1] + \mathcal{A}k_BT\rho\int_{z_{\min}}^{z_{\max}} dz \int d\omega \alpha(z,\omega)\ln 4\pi\alpha(z,\omega), \tag{2.15}$$

where Λ is the thermal wavelength, and we have introduced the integration limits

$$z_{\min} = -\frac{L_z}{2}+\frac{\tilde{\sigma}_T}{2}, \quad z_{\max}=\frac{L_z}{2}-\frac{\tilde{\sigma}_T}{2}. \tag{2.16}$$

The second term in Eq. (2.15) accounts for the loss of entropy in anisotropic configurations [it vanishes for $\alpha(z,\omega)=1/4\pi$].

According to our fluid model, the interaction free energy subdivides into two contributions

$$F^{\mathrm{FF}} = F^{\mathrm{HS}} + \Delta F, \tag{2.17}$$

where F^{HS} constitutes the contribution from the hard sphere (HS) reference fluid [characterized by diameters $\tilde{\sigma}_T$, see Eq. (2.4)]. Due to our homogeneous ansatz (2.8) for the density, F^{HS} can be calculated from the Carnahan-Starling bulk expression [42]

$$\frac{F^{\mathrm{HS}}}{\mathcal{V}} = k_BT\rho\frac{4\eta_T-3\eta_T^2}{(1-\eta_T)^2}, \tag{2.18}$$

where $\eta_T=(\pi/6)\rho\tilde{\sigma}_T^3$ is the packing fraction.

The remaining ("excess") term ΔF appearing in Eq. (2.17) arises from the dipolar and the LJ interactions. Following previous density functional approaches for polar fluids [29,31] we treat these contributions within the modified mean-field (MMF) approximation where the pair distribution function of the system is set to its low-density limit

$$g(\mathbf{r}_1,\omega_1,\mathbf{r}_2,\omega_2) = \exp[-\beta u^{\mathrm{FF}}(\mathbf{r}_{12},\omega_1,\omega_2)]. \tag{2.19}$$

For the present model fluid [see Eq. (2.1)], the pair correlation function is zero for separations $r_{12}<\tilde{\sigma}_T$. The MMF approximation then yields [28–30]

$$\Delta F = -\frac{\rho^2}{2\beta}\int_{r_{12}>\tilde{\sigma}_T} d\mathbf{r}_1 d\mathbf{r}_2 \int d\omega_1 d\omega_2 \times \alpha(z_1,\omega_1)\alpha(z_2,\omega_2)f(\mathbf{r}_{12},\omega_1,\omega_2), \tag{2.20}$$

where

$$f(\mathbf{r}_{12},\omega_1,\omega_2) = \exp[-\beta u^{\mathrm{FF}}(\mathbf{r}_{12},\omega_1,\omega_2)]-1 = \exp[-\beta u^{\mathrm{dip}}(\mathbf{r}_{12},\omega_1,\omega_2)-\beta u^{\mathrm{LJ}}(r_{12})]-1, \quad r_{12}>\tilde{\sigma}_T \tag{2.21}$$

is the Mayer function. Due to the presence of the dipolar interaction (u^{dip}) in the potential function u^{FF} [see Eq. (2.1)], the Mayer function of the present polar fluid is long-ranged since it decays, to leading order, as $-\beta u^{\mathrm{dip}}\propto r_{12}^{-3}$. Following Ref. [31] we therefore isolate the long-ranged (LR) term by rewriting the Mayer function as $f=f^{\mathrm{SR}}+f^{\mathrm{LR}}$, where

$$f^{\mathrm{LR}}(\mathbf{r}_{12},\omega_1,\omega_2) = -\beta u^{\mathrm{dip}}(\mathbf{r}_{12},\omega_1,\omega_2) \tag{2.22}$$

and

$$f^{\mathrm{SR}}(\mathbf{r}_{12},\omega_1,\omega_2) = \exp[-\beta u^{\mathrm{dip}}(\mathbf{r}_{12},\omega_1,\omega_2)-\beta u^{\mathrm{LJ}}(r_{12})] + \beta u^{\mathrm{dip}}(\mathbf{r}_{12},\omega_1,\omega_2)-1 \tag{2.23}$$

contains the remaining short-ranged (SR) contribution. Indeed, as may be easily verified from a Taylor expansion of the exponential $\exp[-\beta u^{\mathrm{dip}}]$ appearing in f^{SR} in powers of the dipolar potential, f^{SR} decays (to leading order) as r_{12}^{-6}. Starting from the Taylor expansion, we further approximate the short-ranged part by keeping only terms up to second order in u^{dip}, yielding

$$f^{\mathrm{SR}}(\mathbf{r}_{12},\omega_1,\omega_2) \approx \{\exp[-\beta u^{\mathrm{LJ}}(r_{12})]-1\} - \beta u^{\mathrm{dip}}(\mathbf{r}_{12},\omega_1,\omega_2)\{\exp[-\beta u^{\mathrm{LJ}}(r_{12})]-1\} + \frac{\beta^2}{2}\exp[-\beta u^{\mathrm{LJ}}(r_{12})][u^{\mathrm{dip}}(\mathbf{r}_{12},\omega_1,\omega_2)]^2. \tag{2.24}$$

The above truncation has been first employed in a MMF study of the surface tension of polar fluids [28]. Later, results for the phase diagrams of bulk polar fluids [31] have indicated that the second-order theory yields data very close to those from the full MMF approximation (without any truncation). From a technical point of view the truncation somewhat simplifies the minimization procedure since it restricts the density expansion coefficients $\alpha_{lm}(z)$ [see Eq. (2.10)] appearing in ΔF to those with $l \leq 2$ and $|m| \leq 2$.

We now consider successively the contributions of the three terms of $f^{\mathrm{SR}}(\mathbf{r}_{12},\omega_1,\omega_2)$ [see Eq. (2.24)] to the short-ranged part of the excess free energy [see Eq. (2.20)] defined as

$$\Delta F^{\mathrm{SR}} = -\frac{\rho^2}{2\beta}\int_{r_{12}>\tilde{\sigma}_T} d\mathbf{r}_1 d\mathbf{r}_2 \int d\omega_1 d\omega_2 \times \alpha(z_1,\omega_1)\alpha(z_2,\omega_2) f^{\mathrm{SR}}(\mathbf{r}_{12},\omega_1,\omega_2). \tag{2.25}$$

Inserting the first term on the right side of Eq. (2.24) into Eq. (2.25), and using the normalization of the orientational distribution [see Eq. (2.9)], one finds

$$\Delta F^{\mathrm{SR,I}} = -\frac{\rho^2}{2\beta}\int_{r_{12}>\tilde{\sigma}_T} d\mathbf{r}_1 d\mathbf{r}_2 \{\exp[-\beta u^{\mathrm{LJ}}(r_{12})]-1\}. \tag{2.26}$$

The spatial integrals can be simplified by introducing cylindrical coordinates $\mathbf{r}_i=(\mathbf{R}_i,z_i)$ $(i=1,2)$, where $\mathbf{R}_i=(R_i,\varphi_i)$ is the projection of $\mathbf{r}_i$ onto the x-y plane ($R_i=\sqrt{x_i^2+y_i^2}$, φ_i is the polar angle). Furthermore, due to the translational invariance of the system in the directions parallel to the walls, the integrations over $\mathbf{R}_1$ and $\mathbf{R}_2$ can be replaced by an integration over the in-plane separation vector $\mathbf{R}_{12}=\mathbf{R}_1-\mathbf{R}_2=(R_{12},\varphi_{12})$, where $R_{12}=\sqrt{(x_1-x_2)^2+(y_1-y_2)^2}$ and $\varphi_{12}=\varphi_1-\varphi_2$. Thus,

$$\int_{r_{12}>\tilde{\sigma}_T} d\mathbf{r}_1 d\mathbf{r}_2 \cdots \to \mathcal{A}\int_{z_{\min}}^{z_{\max}} dz_1 \int_{z_{\min}}^{z_{\max}} dz_2 \times \int_0^{2\pi} d\varphi_{12} \int_{R_{\min}(T)}^{\infty} dR_{12} R_{12} \cdots, \tag{2.27}$$

where the lower integration limit of the radial integral is given by

$$R_{\min}(T) = \begin{cases} 0, & |z_{12}| > \tilde{\sigma}_T, \\ \sqrt{\tilde{\sigma}_T^2-(z_1-z_2)^2}, & |z_{12}| \leq \tilde{\sigma}_T \end{cases} \tag{2.28}$$

with $z_{12}=z_1-z_2$. Combining Eqs. (2.27) and (2.26) we obtain

$$\Delta F^{\mathrm{SR,I}} = -\frac{\rho^2}{2\beta} 2\pi\mathcal{A}\int_{z_{\min}}^{z_{\max}} dz_1 \int_{z_{\min}}^{z_{\max}} dz_2 g_{\mathrm{I}}(z_{12}), \tag{2.29}$$

where we have introduced the function

$$g_{\mathrm{I}}(z_{12}) = \int_{R_{\min}(T)}^{\infty} dR_{12} R_{12}\left\{\exp\left[-\beta u^{\mathrm{LJ}}\left(\sqrt{R_{12}^2+z_{12}^2}\right)\right]-1\right\}. \tag{2.30}$$

The next contribution to the free energy ΔF^{SR} is given by [see Eqs. (2.24) and (2.25)]

$$\Delta F^{\mathrm{SR,II}} = \frac{\rho^2}{2}\int_{r_{12}>\tilde{\sigma}_T} d\mathbf{r}_1 d\mathbf{r}_2 \int d\omega_1 d\omega_2 \alpha(z_1,\omega_1)\alpha(z_2,\omega_2) \times u^{\mathrm{dip}}(\mathbf{r}_{12},\omega_1,\omega_2)\{\exp[-\beta u^{\mathrm{LJ}}(r_{12})]-1\}. \tag{2.31}$$

In order to perform the angular integrations we rewrite the dipole potential in rotationally invariant form

$$u^{\mathrm{dip}}(\mathbf{r}_{12},\omega_1,\omega_2) = -\gamma\frac{\mu^2}{r_{12}^3}\Phi_{112}(\omega_1,\omega_2,\omega_{12}), \tag{2.32}$$

where $\gamma=8\pi\sqrt{2\pi/15}$, $\omega_{12}=(\theta_{12},\varphi_{12})$ describes the orientation of $\mathbf{r}_{12}$, and Φ_{112} is a rotational invariant [41,43] defined as

$$\Phi_{l_1 l_2 L}(\omega_1,\omega_2,\omega_{12}) = \sum_{m_1 m_2 m} C(l_1 l_2 L, m_1 m_2 M) \times \mathcal{Y}_{l_1 m_1}(\omega_1)\mathcal{Y}_{l_2 m_2}(\omega_2)\mathcal{Y}^*_{\mathrm{LM}}(\omega_{12}). \tag{2.33}$$

In Eq. (2.33), the quantities $C(l_1 l_2 L, m_1 m_2 M)$ are Clebsch-Gordan (CG) coefficients [41] which are different from zero only for $|l_1-l_2| \leq L \leq |l_1+l_2|$ and $M=m_1+m_2$. Inserting Eqs. (2.32) and (2.33) into Eq. (2.31), and using the spherical expansion of the orientational distributions given in Eq. (2.10), the angular integrals over ω_1 and ω_2 can be performed making use of the orthogonality of the spherical harmonics [see Eq. (2.13) below]. The remaining spatial integrations in Eq. (2.31) can be simplified by introducing cylindrical variables [see Eq. (2.27)]. We note that the functions $\mathcal{Y}^*_{2M}$ appearing in Φ_{112} [see Eq. (2.33) with $l_1 l_2 L=112$] depend explicitly on the variable φ_{12}. In particular, due to the general relation

$$\int_0^{2\pi} d\varphi_{12}\mathcal{Y}_{LM}(\omega_{12}) \propto \int_0^{2\pi} d\varphi_{12}\exp(iM\varphi_{12}) = 2\pi\delta_{M,0}, \tag{2.34}$$

it is clear that only those terms in the sum in Eq. (2.33), which are characterized by $M=0$, and therefore $m_1 \overset{!}{=} -m_2 = m$, "survive" the spatial integral. We thus obtain

$$\Delta F^{\mathrm{SR,II}} = -\frac{\rho^2}{2} 2\pi \mathcal{A} \gamma \mu^2 \sum_{m=-1}^{1} C(112; m\underline{m}0) \int_{z_{\min}}^{z_{\max}} dz_1 \alpha_{1\underline{m}}(z_1) \times \int_{z_{\min}}^{z_{\max}} dz_2 \alpha_{1m}(z_2) \int_{R_{\min}(T)}^{\infty} dR_{12} R_{12} \times \{\exp[-\beta u^{\mathrm{LJ}}(r_{12})] - 1\} \mathcal{Y}_{20}(\omega_{12}) (R_{12}^2 + z_{12}^2)^{-3/2}. \tag{2.35}$$

The remaining spherical harmonic appearing in Eq. (2.35) is defined as $\mathcal{Y}_{20}(\omega_{12}) = \sqrt{5/4\pi}\mathcal{P}_2(\cos\theta_{12})$, where $\cos\theta_{12} = z_{12}/r_{12} = z_{12}/\sqrt{R_{12}^2 + z_{12}^2}$ and $\mathcal{P}_2(x) = (3x^2 - 1)/2$ is a Legendre polynomial [41]. Introducing the function

$$g_{\mathrm{II}}(z_{12}) = \frac{1}{2}\sqrt{\frac{5}{4\pi}} \int_{R_{\min}(T)}^{\infty} dR_{12} R_{12} \times \left\{\exp\left[-\beta u^{\mathrm{LJ}}\left(\sqrt{R_{12}^2 + z_{12}^2}\right)\right] - 1\right\} \times \left(\frac{3z_{12}^2}{R_{12}^2 + z_{12}^2} - 1\right)(R_{12}^2 + z_{12}^2)^{-3/2}, \tag{2.36}$$

the free energy contribution becomes

$$\Delta F^{\mathrm{SR,II}} = -\frac{\rho^2}{2} 2\pi \mathcal{A} \gamma \mu^2 \int_{z_{\min}}^{z_{\max}} dz_1 \int_{z_{\min}}^{z_{\max}} dz_2 g_{\mathrm{II}}(z_{12}) \times \sum_{m=-1}^{1} C(112, m\underline{m}0) \alpha_{1\underline{m}}(z_1) \alpha_{1m}(z_2). \tag{2.37}$$

The remaining contribution to ΔF^{SR} stems from the third term in the corresponding Mayer function [see Eq. (2.24)] and reads

$$\Delta F^{\mathrm{SR,III}} = -\frac{\beta\rho^2}{4} \int_{r_{12} > \tilde{\sigma}_T} d\mathbf{r}_1 d\mathbf{r}_2 \times \int d\omega_1 d\omega_2 \alpha(z_1, \omega_1) \alpha(z_2, \omega_2) \times [u^{\mathrm{dip}}(\mathbf{r}_{12}, \omega_1, \omega_2)]^2 \exp[-\beta u^{\mathrm{LJ}}(r_{12})]. \tag{2.38}$$

To simplify the integrand we use again Eq. (2.32) relating u^{dip} to the invariant Φ_{112} and apply the product formula for rotational invariants [41]. The latter implies

$$(\Phi_{112})^2 = (8\pi)^{-3/2}\left(a_{000}\Phi_{000} + a_{220}\Phi_{220} + a_{022}\Phi_{022} + a_{202}\Phi_{202} + a_{222}\Phi_{222} + a_{224}\Phi_{224}\right), \tag{2.39}$$

where the constants $a_{000} = 5$, $a_{220} = \sqrt{1/5}$, $a_{202} = a_{022} = 1$, $a_{222} = \sqrt{2/35}$, $a_{224} = 6\sqrt{2/35}$, and the rotational invariants $\Phi_{l_1 l_2 l}$ are defined according to Eq. (2.33). We can now treat the angular and spatial integrals in Eq. (2.38) in the same way as before. Employing Eq. (2.34) and introducing the functions

$$g_{\mathrm{III}}^{(l)}(z_{12}) = \int_{R_{\min}(T)}^{\infty} dR_{12} R_{12} \exp[-\beta u^{\mathrm{LJ}}(r_{12})] \times \mathcal{Y}_{l0}(\omega_{12}) (R_{12}^2 + z_{12}^2)^{-3} \tag{2.40}$$

with $\mathcal{Y}_{l0}(\omega_{12}) = \sqrt{(2l+1)/4\pi}\mathcal{P}_l(\cos\theta_{12})$, we find

$$\Delta F^{\mathrm{SR,III}} = -\frac{\beta\rho^2}{4}(8\pi)^{(-3/2)} 2\pi \mathcal{A} \gamma^2 \mu^2 \int_{z_{\min}}^{z_{\max}} dz_1 \times \int_{z_{\min}}^{z_{\max}} dz_2 \Big[a_{000} g_{\mathrm{III}}^{(0)}(z_{12}) + a_{220} \sum_{m=-2}^{2} C(220, m\underline{m}0) \alpha_{2m}(z_1) \alpha_{2\underline{m}}(z_2) g_{\mathrm{III}}^{(0)}(z_{12}) + a_{202} C(202,000)[\alpha_{00}\alpha_{20}(z_2) + \alpha_{20}(z_1)\alpha_{00}] g_{\mathrm{III}}^{(2)}(z_{12}) + a_{222} \sum_{m=-2}^{2} C(222, m\underline{m}0) \alpha_{2m}(z_1) \alpha_{2\underline{m}}(z_2) g_{\mathrm{III}}^{(2)}(z_{12}) + a_{224} \sum_{m=-2}^{2} C(224, m\underline{m}0) \alpha_{2m}(z_1) \alpha_{2\underline{m}}(z_2) g_{\mathrm{III}}^{(4)}(z_{12}) \Big], \tag{2.41}$$

where we have used that $a_{202} = a_{022}$ and $C(202,000) = C(022,000)$.

Finally, the long-range part of the Mayer function [see Eq. (2.22)] yields the free energy

$$\Delta F^{\mathrm{LR}} = \frac{\rho^2}{2} \int_{r_{12} > \tilde{\sigma}_T} d\mathbf{r}_1 d\mathbf{r}_2 \int d\omega_1 d\omega_2 \times \alpha(z_1, \omega_1) \alpha(z_2, \omega_2) u^{\mathrm{dip}}(\mathbf{r}_{12}, \omega_1, \omega_2). \tag{2.42}$$

The integrand has the same angle-dependence as that appearing in $\Delta F^{\mathrm{SR,II}}$ [see Eq. (2.31)], and one obtains

$$\Delta F^{\mathrm{LR}} = -\frac{\rho^2}{2} 2\pi \mathcal{A} \gamma \mu^2 \sum_{m=-1}^{1} C(112, m\underline{m}0) \times \int_{z_{\min}}^{z_{\max}} dz_1 \alpha_{1\underline{m}}(z_1) \int_{z_{\min}}^{z_{\max}} dz_2 \alpha_{1m}(z_2) \times \int_{R_{\min}(T)}^{\infty} dR_{12} R_{12} \mathcal{Y}_{20}(\omega_{12}) (R_{12}^2 + z_{12}^2)^{-3/2}. \tag{2.43}$$

The integral over the in-plane separation R_{12} can be evaluated analytically, yielding

$$g_{\mathrm{LR}}(z_{12}) \equiv \frac{1}{2}\sqrt{\frac{5}{4\pi}}\int_{R_{\min}(T)}^{\infty} dR_{12}R_{12} \times \left(\frac{3z_{12}^2}{R_{12}^2+z_{12}^2}-1\right)(R_{12}^2+z_{12}^2)^{-3/2} = \begin{cases} 0, & |z_{12}| > \tilde{\sigma}_T, \\ \sqrt{\frac{5}{16\pi}}(z_{12}^2-\tilde{\sigma}_T^2)/\tilde{\sigma}_T^3, & |z_{12}| \le \tilde{\sigma}_T, \end{cases} \tag{2.44}$$

where we have used Eq. (2.28) and the explicit formula for $\mathcal{Y}_{20}(\omega_{12})$ given below Eq. (2.35). Combining Eqs. (2.44) and (2.43) we arrive at the expression

$$\Delta F^{\mathrm{LR}} = -\frac{\rho^2}{2}2\pi\mathcal{A}\gamma\mu^2\sum_{m=-1}^{1} C(112,m\underline{m}0) \times \int_{z_{\min}}^{z_{\max}} dz_1\alpha_{1\underline{m}}(z_1)\int_{z_{\min}}^{z_{\max}} dz_2\alpha_{1m}(z_2)g_{\mathrm{LR}}(z_{12}). \tag{2.45}$$

Finally, collecting all terms, the full density functional within the present approximations reads

$$\frac{\Omega[\rho]}{\mathcal{V}} = k_BT\rho[\ln(\rho\Lambda^3)-1]-\mu_{\mathrm{chem}}\rho + k_BT\frac{\rho}{L_z-\tilde{\sigma}_T}\int_{z_{\min}}^{z_{\max}} dz\int d\omega\alpha(z,\omega)\ln 4\pi\alpha(z,\omega) + k_BT\rho\frac{4\eta_T-3[\eta_T]^2}{[1-\eta_T]^2} + \frac{1}{\mathcal{V}}(\Delta F^{\mathrm{SR,I}}+\Delta F^{\mathrm{SR,II}}+\Delta F^{\mathrm{SR,III}}+\Delta F^{\mathrm{LR}})+\frac{F^{\mathrm{FW}}}{\mathcal{V}}, \tag{2.46}$$

where the excess free energy terms are defined according to Eqs. (2.29), (2.37), (2.41), and (2.45), respectively, and

$$\frac{F^{\mathrm{FW}}}{\mathcal{V}} = \frac{\rho}{L_z-\tilde{\sigma}_T}\int_{z_{\min}}^{z_{\max}} dzu^{\mathrm{FW}}(z) = -\frac{2\pi\rho\sigma^3}{3}\epsilon_{\mathrm{FF}}\frac{16L_z}{\tilde{\sigma}_T^2(\tilde{\sigma}_T-2L_z)^2} \tag{2.47}$$

is the external contribution.

3. Euler-Lagrange equations

Within our ansatz (2.8) for the singlet density, the Euler-Lagrange equation (2.7) decouples into two parts

$$\frac{\partial\Omega}{\partial\rho}=0, \qquad \frac{\delta\Omega}{\delta\alpha(z,\omega)}=0. \tag{2.48}$$

Employing the functional (2.46), the first member of Eq. (2.48) yields the condition

$$\ln\rho = \beta\mu_{\mathrm{chem}} - \ln\lambda^3 - \frac{1}{L_z-\tilde{\sigma}_T}\int_{z_{\min}}^{z_{\max}} dz\int d\omega\alpha(z,\omega)\ln 4\pi\alpha(z,\omega) - \frac{\partial}{\partial\rho}\left(\frac{\beta F^{\mathrm{HS}}}{\mathcal{V}}+\frac{\beta\Delta F}{\mathcal{V}}\right)+\frac{2\pi}{3}\epsilon_{\mathrm{FF}}\frac{16L_z\sigma^3}{\tilde{\sigma}_T^2(\tilde{\sigma}_T-2L_z)^2}. \tag{2.49}$$

The minimization with respect to the orientational distribution $\alpha(z,\omega)$ has to be performed obeying the norm condition in Eq. (2.9). Solving the resulting expression with respect to the orientational parameters $\alpha_{lm}(z)$ [see Eq. (2.11)] one obtains

$$\alpha_{lm}(z) = \frac{1}{N(z)}\int d\omega\mathcal{Y}_{lm}^*(\omega)\exp[I(z,\omega)], \tag{2.50}$$

where $N(z)=\int d\omega\exp[I(z,\omega)]$ is the normalization factor and the exponent in the distribution is given by

$$I(z,\omega) = \rho\beta\mu^2\gamma 2\pi\sum_{m=-1}^{1}(-1)^m C(112;m\underline{m}0)\mathcal{Y}_{1m}(\omega)\int_{z_{\min}}^{z_{\max}} dz_2\alpha_{1\underline{m}}(z_2)(g_{\mathrm{II}}(\tilde{z})+g_{\mathrm{LR}}(\tilde{z})) + \frac{\beta^2\rho^2}{2}(8\pi)^{(-3/2)}2\pi\gamma^2\int_{z_{\min}}^{z_{\max}} dz_2\Bigg[a_{220}\sum_{m=-2}^{2}(-1)^m C(220,m\underline{m}0)\mathcal{Y}_{2m}(\omega)\alpha_{2m}(z_2)g_{\mathrm{III}}^{(0)}(\tilde{z}) + a_{202}C(202,000)(4\pi)^{-1/2}[\alpha_{20}(z_2)+\mathcal{Y}_{20}(\omega)]g_{\mathrm{III}}^{(2)}(\tilde{z}) + a_{222}\sum_{m=-2}^{2}C(222,m\underline{m}0)(-1)^m\mathcal{Y}_{2m}(\omega)\alpha_{2m}(z_2)g_{\mathrm{III}}^{(2)}(\tilde{z}) + a_{224}\sum_{m=-2}^{2}C(224,m\underline{m}0)(-1)^m\mathcal{Y}_{2m}(\omega)\alpha_{2m}(z_2)g_{\mathrm{III}}^{(4)}(\tilde{z})\Bigg], \tag{2.51}$$

where we have introduced the variable $\tilde{z}=z-z_2$.

4. Phase equilibria

One main focus of the present work is to explore the influence of confinement on the overall phase behavior of the polar fluid. This requires simultaneous solution of the Euler-Lagrange equations (2.49) and (2.50) for a wide range of temperatures and chemical potentials, which, given the z dependence of the orientational order parameters, would be a time-consuming task. In order to get a first overview we make one further approximation, that is

$$\alpha_{lm}(z) = \alpha_{lm}. \tag{2.52}$$

With this assumption the free energy functional (2.46) becomes a function of the (average) number density ρ and the eight nontrivial orientational parameters $\alpha_{l,m}$ characterized by $0<l\leq 2$. Moreover, as shown in Appendix A, the integrations required in the evaluation for the long-range part of the free energy [see Eq. (2.45)] can be performed analytically, yielding

$$\frac{\Delta F^{\mathrm{LR}}}{\mathcal{V}} = -\rho^2\mu^2\frac{4\pi^2}{3(L_z-\tilde{\sigma}_T)}\left(-\frac{4L_z}{3}+\frac{11\tilde{\sigma}_T}{6}\right)(\alpha_{10}^2-|\alpha_{11}|^2). \tag{2.53}$$

Equation (2.53) can be rewritten by introducing the components of the (homogeneous) polarization $\mathbf{P}$ [see Eqs. (2.12) and (2.13)], which gives

$$\frac{\Delta F^{\mathrm{LR}}}{\mathcal{V}} = -\rho^2\mu^2\frac{4\pi}{3}\frac{L_z}{L_z-\tilde{\sigma}_T}\left(1-\frac{11\tilde{\sigma}_T}{8L_z}\right)\left(\frac{1}{2}(P_x^2+P_y^2)-P_z^2\right). \tag{2.54}$$

Equation (2.53) reveals that, as long as $L_z/\tilde{\sigma}_T > 11/8 \approx 1.4$, ΔF^{LR} is negative (positive) if $|P_{x(y)}|>0$ ($|P_z|>0$). In other words, the long-range dipolar interactions favor polarization parallel to the confining walls whereas perpendicular orientation is unfavorable. This result is consistent with macroscopic electrostatics which states that, in an infinitely extended slab (homogeneous) polarization normal to the surfaces yields surface charges, which in turn generate a depolarizing field (see, e.g., Ref. [37]). Perpendicular polarization is therefore energetically unfavorable and, in fact, real systems would avoid this situation by the formation of domains which is not captured by the present approach [see Eq. (2.8)]. On the other hand, the surface charges (and the depolarizing field) are absent if the system polarizes parallel to the walls [37]. Interestingly, from the macroscopic perspective, these results do not depend on the wall boundary conditions, that is on the dielectric constant ϵ_{wall} of the walls (the present model implicitly assumes *insulating* walls with $\epsilon_{\mathrm{wall}}=1$). Indeed, one can show that even for the case of "conducting" walls ($\epsilon_{\mathrm{wall}}=\infty$), where additional "image" interactions need to be considered [44], the system develops in-plane polarization.

With Eq. (2.52), the Euler-Langrange equations (2.49) and (2.50) can be solved numerically by employing a multidimensional Newton-Raphson algorithm, yielding the equilibrium configuration for given $(\mu_{\mathrm{chem}},T,\mathcal{V})$. In order to identify coexisting states at given chemical potential μ_{chem}, we combine Eqs. (2.49) and (2.50) with a further equation reflecting that the pressures $p=-\Omega^{\mathrm{eq}}(\mu_{\mathrm{chem}},T)/\mathcal{V} = -\Omega[\rho^{\mathrm{eq}},\alpha^{\mathrm{eq}}(\omega)]/\mathcal{V}$ of both states have to be equal as well.

5. The limit $L_z\to\infty$

Within the present model of confinement, one expects the bulk behavior to be recovered by taking the limit $L_z\to\infty$ of the density functional expressions discussed so far. However, inspection of Eq. (2.53) shows that the differences in ΔF^{LR} between parallel and perpendicular ordering persist in this limit, which is clearly unphysical when we consider an infinite (bulk) system without (or with conducting) boundaries. This feature is again a well-known consequence of the long-range character of the dipolar interactions and can be attributed to our cylindrical evaluation of the relevant integrals in Eq. (2.42). To overcome these problems we perform the calculations for bulk fluids using a slightly different density functional [31] where the ordering direction is predefined to be along the z axis. This corresponds to the simpler density expansion

$$\rho^b(\mathbf{r},\omega) = \rho\alpha(\cos\theta) = \rho\sum_l \alpha_l^b\mathcal{P}_l(\cos\theta), \tag{2.55}$$

where θ is the angle relative to the z axis. The resulting density functional is given in Appendix B. We note that the long-range part of the bulk free energy $\Delta F^{b,\mathrm{LR}}$ [see Eq. (B3)] is evaluated under the assumption that the polarization in the z direction does not induce any depolarizing field [31] [any other choice would be inconsistent with our ansatz (2.55)]. Therefore, Eq. (B3) is consistent with Eq. (2.54), if we assume polarization along an arbitrary direction parallel to the walls and then take the limit $L_z\to\infty$.

III. RESULTS AND DISCUSSION

The state of the Stockmayer fluid can be characterized by the reduced (average) density $\rho^*=\rho\sigma^3$, the reduced chemical potential $\mu^*_{\mathrm{chem}}=\epsilon_{\mathrm{FF}}^{-1}[\mu_{\mathrm{chem}}-3k_BT\ln(\lambda/\sigma)]$, the reduced temperature $\tau=k_BT/\epsilon_{\mathrm{FF}}$, and the reduced dipole moment $m^*=\mu/\sqrt{\epsilon_{\mathrm{FF}}\sigma^3}$, where m^{*2} measures the strength of dipolar interactions in an antiparallel side-by-side configuration (and contact of the spheres) relative to spherical (LJ) interactions. Due to the additional hard core of our present Stockmayer model [see Eq. (2.1)], it transforms directly into the DHS fluid ($u_{\mathrm{LJ}}=\epsilon_{\mathrm{FF}}=0$) upon taking the limit $m^*\to\infty$. *In* this limit, the temperature is described by the parameter $T^*=k_BT\sigma^3/\mu^2$, and the reduced chemical potential $\mu^*_{\mathrm{chem}}=\sigma^3/\mu^2[\mu_{\mathrm{chem}}-3k_BT\ln(\lambda/\sigma)]$.

In the following we first discuss the impact of confinement on the overall phase behavior which, as we will show, strongly depends on the relative strength of the dipolar interactions. In fact, calculating phase diagrams for a range of values of m^* it turns out that one can distinguish three regimes of dipole moments which differ in the types of phase behavior encountered upon decreasing the wall separation from the bulk limit $L_z\to\infty$. The corresponding phase diagrams will be discussed in the next three paragraphs, where we employ both the (average) density-temperature- and the chemical potential-temperature plane. The latter representa-

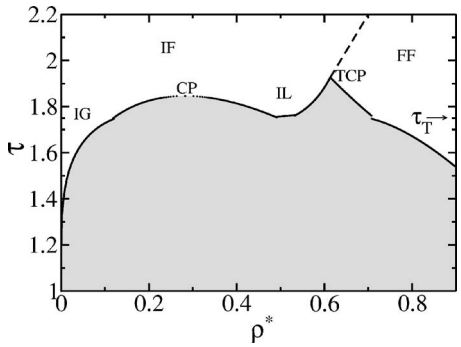

FIG. 1. Phase diagram of a bulk Stockmayer fluid at $m^*=1.5$ in the density-temperature plane. Gray regions indicate two- or three-phase coexistence regions, and the dashed line stands for a line of critical points. For further explanation of the lines and symbols, see main text.

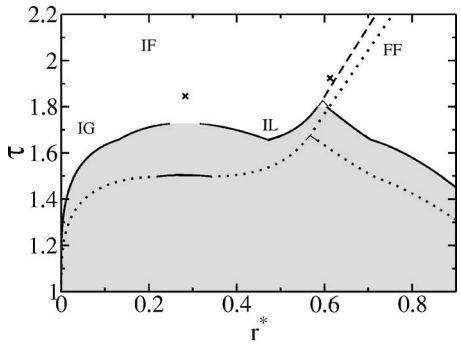

FIG. 2. Density-temperature phase diagrams of confined Stockmayer fluids ($m^*=1.5$) at $L_z^*=10$ (solid/dashed lines) and $L_z^*=4$ (dotted lines). The crosses indicate the critical and tricritical temperatures of the corresponding bulk system (see Fig. 1).

tion is closer to typical sorption experiments of confined fluids [45] where the chemical potential (rather than the average density) of the pore fluid is fixed by allowing the pore fluid to exchange particles with a bulk reservoir. The last part of this section then deals with the *local* orientational structure obtained by minimization of the density functional at specific state points.

A. Phase behavior

1. Moderate dipole moments

We start by considering a Stockmayer fluid characterized by the dipole moment $m^*=1.5$, which is a typical value for moderately polar molecular fluids such as chloroform [14]. Density functional results for the corresponding bulk phase diagram in the fluid phase regime are shown in Fig. 1. At low and intermediate densities, and above the triple temperature τ_T, the system behaves essentially van der Waals–like in that the isotropic high-temperature fluid (IF), characterized by zero orientational order parameters ($\alpha_{l>0}^b=0$), separates into an isotropic gas (IG) and an isotropic liquid (IL) below the vapor-liquid critical temperature τ_{CP}. The dipolar interactions affect this transition merely as an additional attraction, as reflected by the fact that the critical temperature is somewhat larger than the corresponding one of the pure LJ-like fluid [$\tau_{CP}(m^*=0)\approx 1.33$ within the present approximations]. Upon compression of the IL phase the dipolar interactions dominate the phase behavior and one observes a transition into a ferroelectric fluid (FF) phase with $\alpha_{l\geq 1}^b>0$. At temperatures below τ_{CP} the IL-FF transition is characterized by jumps both in density and in the orientational order parameters. The same is true for the IG-FF transition appearing below the IG-IL-FF triple temperature τ_T. On the other hand, increasing τ towards the tricritical temperature τ_{TCP} the differences between isotropic and ferroelectric phases vanish, and for temperatures above τ_{TCP} the IF-FF transition becomes continuous in all order parameters, resulting in a line of (ferroelectric) critical points $\tau_{FCP}(\rho_{FCP}^*)$. These points can be calculated from a Landau expansion of the density functional as demonstrated in an earlier MMF study [31] on bulk Stockmayer fluids. The present results are, in fact, very close to those in Ref. [31], the remaining small differences stemming from our truncation of the expansion of the Mayer function. Compared to computer simulation results of Stockmayer fluids [15–17], it turns out that the MMF theory correctly predicts the phase behavior on qualitative level even though the ferroelectric transition temperatures are seriously overestimated, as one might have expected in view of the mean-field character of the theory.

We now discuss the influence of confinement. Two exemplary phase diagrams are shown in Fig. 2 corresponding to the wall separations $L_z^*=L_z/\sigma=10$ and $L_z^*=4$, respectively. At both degrees of confinement, the phases occurring in the diagrams are the same as in the bulk, a special feature of ferroelectric phase of the confined systems being that the director characterizing the spontaneous polarization points along an (arbitrary) direction parallel to the confining walls. This restriction, which lifts the three-dimensional degeneracy of the corresponding bulk ordering direction, can be explained by macroscopic arguments as described in Sec. II B 4. Apart from this feature one concludes from Fig. 2 that, for the moderate dipole moment and the two pore widths considered, confinement does not change the topology of the phase diagrams, but does have a profound influence on the location of the critical, tricritical, and triple points. For a more detailed comparison we have indicated the bulk CP and TCP by crosses in the phase diagrams in Fig. 2. Considering first the vapor-liquid critical points one observes that, upon decreasing L_z^*, the critical temperature also decreases to values significantly smaller than $\tau_{CP,bulk}$. This is a well-known feature of the condensation transition of confined fluids, which has been studied in detail (theoretically and by simulation) also for simpler systems such as confined LJ fluids [3]. As to the critical density, the results in Fig. 2 suggest that ρ_{CP}^* is essentially unaffected by the degree of confinement. However, care has to be taken in interpreting this finding since it is well established that the average density appearing in Fig. 2 is not a suitable order parameter in a confined system. Therefore, we switch to the chemical potential-temperature plane, which allows a more direct comparison between bulk and confined systems. Corresponding phase diagrams (for $L_z^*=4,10,\infty$) are presented in Fig. 3, from which it is seen that not only τ_{CP}, but also the corresponding chemical potential decreases when the confinement becomes more and more

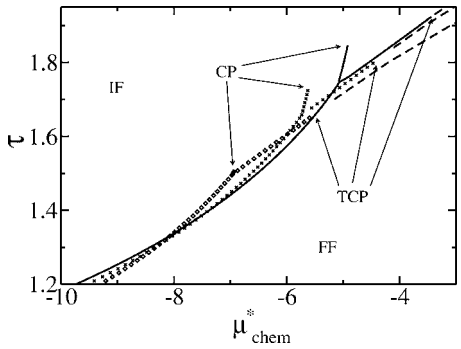

FIG. 3. Phase diagrams for bulk and confined Stockmayer fluids at $m^*=1.5$ in the chemical potential-temperature plane. The solid lines, crosses, and squares indicate first-order transition lines corresponding to the bulk fluid $L_z^*=10$ and $L_z^*=4$. Dashed lines denote the lines of IF-FF critical points.

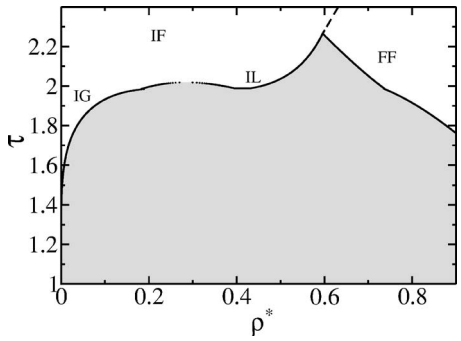

FIG. 4. Phase diagram of a bulk Stockmayer fluid at $m^*=1.65$ in the density-temperature plane. Symbols as in Fig. 1.

severe. This is the so-called capillary condensation typical for confined systems exposed to attractive fluid-wall interactions. Indeed one observes from Fig. 3 that, at a fixed intermediate temperature (above the IG-IL-FF triple temperature at $L_z^*=4$), the confined isotropic gas actually condenses into the isotropic liquid at smaller chemical potentials (and, correspondingly, at smaller pressures) than its bulk counterpart. Interestingly, one finds an analogous behavior to occur with respect to the tricritical point related to the upper (lower) limit of the first-order (second-order) IF-FF transition (see also Figs. 1 and 2). Indeed, as seen from Fig. 3, the tricritical temperatures decrease with increasing confinement, and so do the related chemical potentials. As a consequence there is a small range of temperatures (and chemical potentials) where, at fixed τ (or μ^*_{chem}, respectively), the confined systems actually order already at lower chemical potentials (higher temperatures) than the bulk fluid. This shows that confinement can, in some cases, *support* the onset of ferroelectric ordering. Opposite behavior occurs at very high temperatures above the coexistence regimes, and at temperatures below the triple points where the systems transform directly from the IG into the FF phase (see Figs. 1 and 2). Comparing (at fixed τ) the chemical potentials related to these strong first-order transitions one observes a shift towards larger values indicating that the development of orientational ordering is suppressed rather than promoted here.

2. Larger dipole moments

We now turn to a Stockmayer fluid with somewhat stronger dipolar interactions characterized by the (still realistic) reduced dipole moment $m^*=1.65$. Figure 4 shows the corresponding bulk density-temperature phase diagram, which clearly has the same topology as the corresponding one obtained at $m^*=1.5$ (see Fig. 1). Indeed, the main effect of the increase of m^* consists in a corresponding increase of the vapor-liquid and ferroelectric (tri)critical temperatures. Both effects are expected when the dipolar interactions become more and more important as compared to the spherical attractive interactions. In the present context, the interesting aspect of the phase behavior at $m^*=1.65$ is that there is a stronger competition between the vapor-liquid transition, on one hand, and the isotropic-to-ferroelectric transition, on the other hand, as reflected by the smaller range of temperatures where the isotropic liquid phase is stable. Thus, one may suspect that the IL phase disappears completely when the system is exposed to spatial confinement, which tends to reduce the condensation critical point anyway. That such a scenario can indeed occur can be seen from Fig. 5 where we have plotted the ρ^*-τ diagrams at two different wall separations $L_z^*=10$ and $L_z^*=4$. It is seen that already at $L_z^*=10$ [see Fig. 5(a)], which may be considered as a "mesoscopic" pore width, the vapor-liquid critical point has nearly disappeared. The ferroelectric phase, on the other hand, still occupies a large portion of the parameter space. Finally, upon decreasing the wall separation even further the IL phase becomes entirely suppressed as a thermodynamically stable phase, and

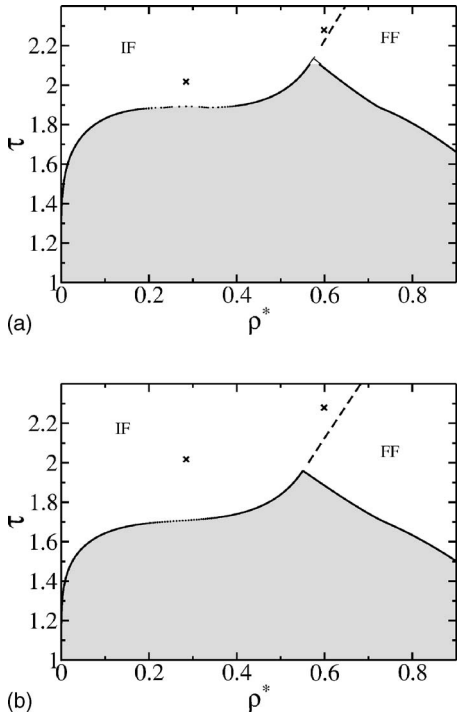

FIG. 5. Density-temperature phase diagrams of confined Stockmayer fluids at $m^*=1.65$ and $L_z^*=10$ (a), $L_z^*=4$ (b). Crosses indicate the critical and tricritical temperatures of the corresponding bulk system (see Fig. 4).

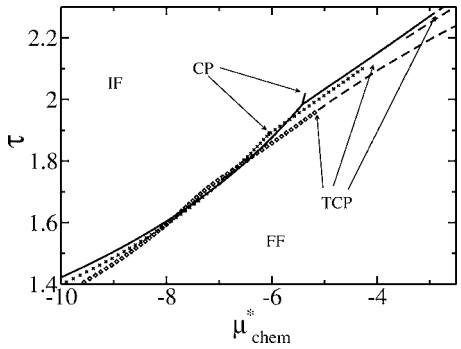

FIG. 6. Same as Fig. 3 but for $m^*=1.65$.

one is left with an IF-FF transition. Corresponding μ^*_{chem}-τ diagrams are plotted in Fig. 6. Apart from the disappearance of the isotropic liquid phase, these diagrams also show that the isotropic-to-ferroelectric transition in the confined fluids is generally shifted to larger chemical potentials (lower temperatures) compared to their bulk counterparts. One thus concludes that at large dipole moments such as $m^*=1.65$ confinement tends to inhibit both the condensation and the isotropic-ferroelectric transition. However, since the impact on the condensation transition is larger, it is the IF-FF transition which "resists" the spatial confinement even under severe conditions.

3. The limit $m^* \to \infty$

For completeness, we finally consider the phase behavior of a "dipole-dominated" system with vanishing LJ interactions, that is, $m^* \to \infty$ (DHS). The corresponding bulk phase diagram plotted in Fig. 7 reveals that the DHS fluid does not exhibit a condensation transition (within the isotropic phase) even in the absence of confinement. This MMF result is consistent with the absence of an ordinary liquid phase in computer simulations of DHS fluids [18,19]. What is neglected within the MMF theory is the dipolar chain and network formation observed in numerous simulation studies of dilute, strongly coupled DHS (see Ref. [19], and references therein). On the other hand, spontaneously polarized phases are predicted in qualitative agreement with the simulation results [46].

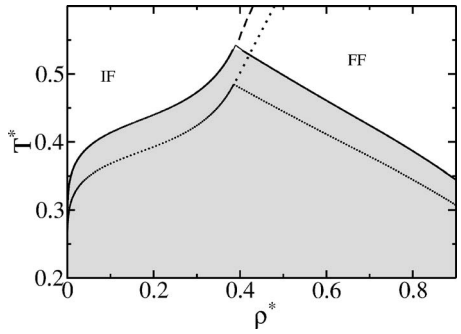

FIG. 7. Phase diagram of the bulk DHS fluid (solid lines) and a corresponding confined system at $L^*_z=4$ (dotted lines) in the density-temperature plane.

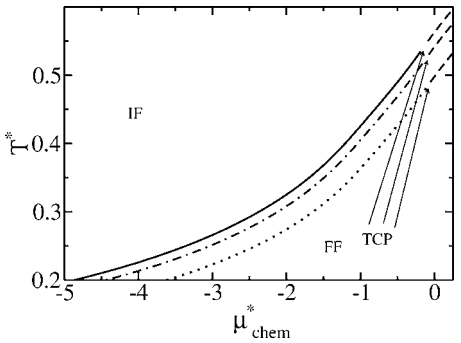

FIG. 8. Phase diagrams of bulk and confined DHS fluids in the chemical potential-temperature plane. The solid, dot-dashed, and dotted lines indicate the IF-FF first-order transition line corresponding to the bulk fluid, $L^*_z=10$ and $L^*_z=4$. Dashed lines denote the lines of IF-FF critical points.

The impact of spatial confinement is illustrated by the set of dotted lines in Fig. 7, which refer to a confined DHS fluid at $L^*_z=4$. Figure 8 contains the corresponding phase diagrams in the chemical potential-temperature plane. As expected from our Stockmayer results discussed in Sec. III A 2, the introduction of confining walls in the system does not change the topology of the bulk phase diagram but shifts the actual conditions under which the IF-FF transition occurs. In particular, the data plotted in Fig. 8 indicate a shift towards larger chemical potentials and lower temperatures compared to the bulk. This finding contradicts, to some extent, results from an earlier study by us [12] where we used a pure MF theory to investigate the IF-FF transition in a DHS like fluid at a fixed temperature. In that study, we came to the conclusion that the transition is actually supported by the confining walls in that the average transition densities (at fixed T^*) are somewhat lower. We note, however, that the MF results in Ref. [12] are based on the assumption that the dipole orientations are completely restricted to directions parallel to the walls already in the isotropic phase. This is a strongly idealized picture, as we will show explicitly in Sec. III B. Finally, it is interesting that the chemical potentials related to the tricritical points in the DHS fluids exhibit a shift towards larger values with decreasing L_z, which is opposite the behavior found in the strongly coupled Stockmayer fluid (see Sec. III A 2). We understand this difference as a consequence of the different fluid-wall interactions, which are attractive in the Stockmayer case, but purely repulsive for the confined DHS fluids considered here.

B. Local orientational structure

So far we have focused on the overall phase behavior, as characterized by the homogeneous parameters ρ^* and $\alpha_{l\geq 1,m}$. It is clear, however, that of all these quantities are, in general, inhomogeneous (i.e., z dependent) due to the presence of confining walls. A prominent effect is the formation of layers (parallel to the walls), which is reflected by oscillations in the local density $\rho(z)$ (see, e.g., Ref. [20]). The purpose of this paragraph is to show that, despite the simplified (constant) number density, the present theory still predicts inho-

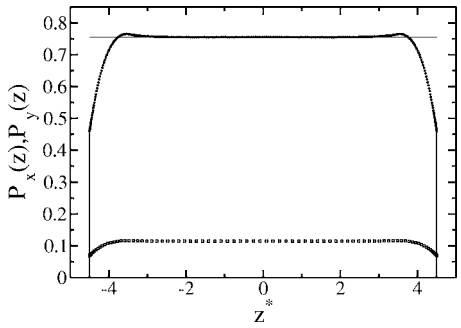

FIG. 9. Components of the local polarization in the x direction (solid line) and y direction (dotted) within the ferroelectric phase of a confined Stockmayer fluid at $m^*=1.5$ and $L_z^*=10$ ($\tau=1.68$, $\rho^*=0.879$).

mogeneous orientational order parameters when we solve Eqs. (2.49) and (2.50) at fixed chemical potentials and temperatures corresponding to specific state points. These calculations have been performed by supplementing the Newton-Raphson algorithm for the equilibrium density by an iteration algorithm for the local order parameters.

We start with the polarization $\mathbf{P}(z)$ characterizing the ferroelectric phase, taking the Stockmayer fluid at $m^*=1.5$ and $L_z^*=10$ as an example [see Fig. 2(a) for the overall phase diagram]. Figure 9 shows typical polarization profiles deep in the FF phase as functions of the reduced distance from the walls, $z^*=z/\sigma$. As expected, the director of the systems points along a direction $\mathbf{d}$ within the x-y plane [i.e., $P_z(z)=0$], where $\mathbf{d}$ is close (but not exactly parallel) to the x axis, therefore both $P_x(z)$ and $P_y(z)$ are different from zero. Due to the hard core of the fluid-wall potential [see Eq. (2.5)], the polarization vanishes for separations $L_z/2 \geq |z| > (L_z-\tilde{\sigma}_T)/2$. Decreasing then $|z|$, the polarization does not directly jump to high values, as one might have expected in view of the hard core (and the otherwise attractive character) of the fluid-wall interaction. Rather, it increases smoothly from an intermediate value directly at the hard core up to a (small) maximum. The soft increase may be interpreted such that the mean field favoring the ferroelectric ordering is reduced in the vicinity of the walls, which seems plausible since the number of neighbors of each particle is reduced here. Furthermore, the small maxima in $P_x(z)$ may be understood as fingerprints of the layer formation, which we have otherwise

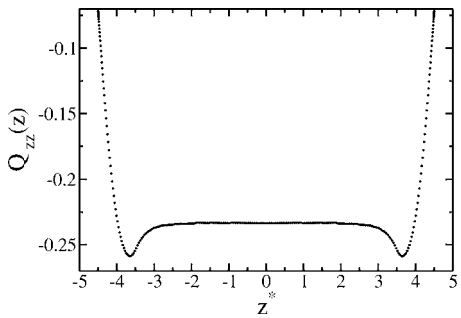

FIG. 10. Local order parameter $Q_{zz}(z)$ within the ferroelectric phase of a confined Stockmayer fluid (same parameters as in Fig. 9).

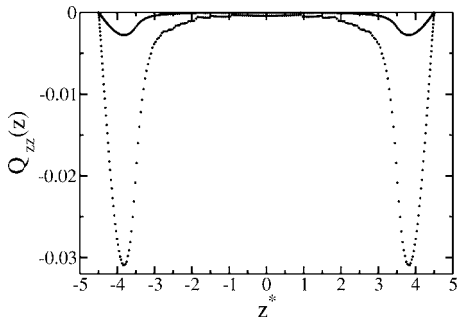

FIG. 11. Local order parameter $Q_{zz}(z)$ within the isotropic gas phase (solid line, $\rho^*=0.042$) and the isotropic liquid phase (dotted line, $\rho^*=0.44$) of a confined Stockmayer fluid at $m^*=1.5$, $L_z^*=10$, and $\tau=1.68$.

suppressed by assuming a homogeneous number density. Finally, for even larger separations from the wall (i.e., in the pore center), one sees from Fig. 9 that $P_x(z)$ and $P_y(z)$ are essentially constant. This feature is, in fact, not too unrealistic in view of the fairly large pore width considered. We also note that the value of $P_x(z)$ in the pore middle is very close to that obtained via a minimization of the density functional under the assumption of homogeneous orientational order parameters. The latter value is indicated by the horizontal line in Fig. 9.

A further interesting quantity is the parameter $Q_{zz}(z)$ defined in Eq. (2.14). Numerical results for this function (again within the FF phase) are shown in Fig. 10. It is seen that $Q_{zz}(z)$ is negative everywhere, reflecting the ordering parallel to the walls. One also observes two minima in $Q_{zz}(z)$ at the same positions z where $\mathbf{P}_x(z)$ exhibits maxima (see Fig. 9), indicating that the tendency of the walls to align the particles is strongest here.

Finally, it is interesting to see that the present theory predicts weak ordering of the dipole axis already in the globally isotropic phase. This can be seen from Fig. 11, where we have plotted results for $Q_{zz}(z)$ in the coexisting IG and IL phases for the same system discussed before ($L_z^*=10$). Clearly, dipole orientations in the z direction are somewhat suppressed already at these low densities, even though the phenomenon is restricted to the "layer" closest to the walls. A stronger local ordering occurs when the confinement becomes more severe, see Fig. 12 for an representative ex-

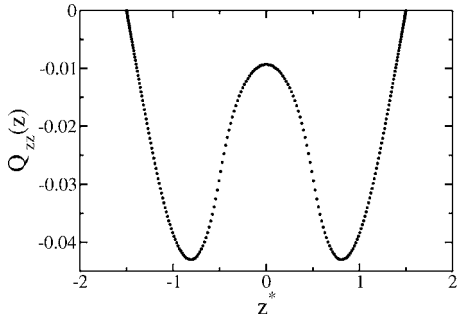

FIG. 12. Local order parameter $Q_{zz}(z)$ within the isotropic liquid phase ($\rho^*=0.477$) of a confined Stockmayer fluid at $m^*=1.5$, $L_z^*=10$, and $\tau=1.55$.

ample at $L_z^*=4$. The data reveal "layer formation" and a resulting restriction of dipole orientations throughout the pore. These density functional results are consistent, on a qualitative level, with computer simulation results for confined Stockmayer [48] and dipolar soft sphere [12] fluids. Quantitatively, the actual magnitude of $Q_{zz}(z)$ is underestimated as compared to typical values observed in the simulation studies, which may be traced back to the MMF approximation of the dipolar correlations. We note, however, that a pure MF theory (where the pair correlations are set to unity) would not predict any local ordering at all.

IV. CONCLUSIONS

In this work we have explored the fluid-fluid phase behavior and the orientational structure of confined polar fluids with different dipole moments by means of density functional theory. Our functional involves two key approximations, that is homogeneity of the local density throughout the pore space, and a (truncated) modified mean-field (MMF) approximation for the intermolecular correlations. The main findings of this work can be summarized as follows.

(1) Confined Stockmayer fluids with small to moderate dipole moments m^* exhibit a gas-liquid critical point separating two isotropic phases, as do their bulk counterparts. The critical temperature τ_{CP} of the confined systems is lowered with respect to the bulk, in accordance to the behavior found in simpler fluids with spherical attractive interactions [4]. On the other hand, for given pore width, τ_{CP} increases with m^* (within the range considered), which is in accordance to what is found in bulk Stockmayer fluids [14] and indicates that the dipolar interactions induce an overall attraction. Moreover, in presence of adsorbing walls, the systems condense at *lower* chemical potentials (capillary condensation). Additional calculations with repulsive walls (not reported in Sec. III) indicated that in this case the condensation occurs at higher chemical potentials (capillary evaporation) whereas the density-temperature phase diagrams remain essentially unchanged. Finally, ferroelectric phases only occur at high densities, with the ferroelectric (tri)critical temperatures being somewhat smaller than in the bulk, but less reduced than those corresponding to the capillary condensation.

(2) An increase of the dipole moment enhances the tendency of the systems to develop ferroelectric phases and can lead to a suppression of the isotropic liquid as a globally stable phase when the confinement becomes sufficiently severe.

(3) In the limit $m^*\to\infty$ (DHS) confinement does not change the overall phase behavior. The ferroelectric tricritical point is shifted to lower temperatures and larger chemical potentials, which might be due to the fact that the walls are purely repulsive for this model.

(4) Despite the basic assumption of a constant pore density, the local polarization $\mathbf{P}(z)$ within the ferroelectric confined fluids is inhomogeneous. In particular, the polarization close to the substrates is strongly reduced (as opposed to the pore center), reflecting the reduced mean field close to the pore walls. This reduction of local order is somewhat reminiscent [6] of the behavior of various real confined fluids such as benzene in mesoporous silica [47] close to their freezing transition where the fluid in the pore center is already solidified, whereas the contact layer is still liquid. In the latter case, however, it is rather the nature of fluid-wall interactions (such as hydrogen bonds) which reduces the local crystalline order in the contact layer whereas in the present model fluid, geometry alone is responsible for reduced ordering field.

(5) The present theory predicts formation of "layers" with local orientational ordering of the dipole axes $[Q_{zz}(z)\neq 0]$ already in isotropic phases. This behavior agrees qualitatively with computer simulations [12,13,48].

It is clear that the present results should rather be seen as predictions on a qualitative level than as accurate quantitative estimates. In particular, the MMF approximation of the correlations is known to overestimate the stability of ferroelectric phases already in bulk polar fluids. We thus expect that features such as confinement-induced suppression of the isotropic liquid (in favor of ferroelectric phases) occur at significantly higher dipole moments compared to the one discussed here ($m^*=1.65$). Also, the assumption of constant number density is known to induce shortcomings (such as inability to predict the correct dependence of τ_{CP} on the pore width) even in simpler (van der Waals–like) models [4]. The confinement-induced oscillations of the real number density could be incorporated, at least approximately, by using more sophisticated expressions such as Rosenfeld's fundamental measure theory (FMT) for the hard-sphere part of the excess free energy [49]. Combining then the FMT functional with the present theory for the dipolar part of the free energy one could construct an improved functional to describe structure and phase behavior of confined polar fluids. Another important task is generalization of the theory to the case of *one* wall and investigation of the related questions of surface-induced order and wetting. Work in these directions is in progress.

ACKNOWLEDGMENTS

We gratefully acknowledge financial support from the Deutsche Forschungsgemeinschaft through the Sonderforschungsbereich 448 "Mesoscopically structured composites" (project B6) and the Emmy-Noether Programme.

APPENDIX A: LONG-RANGED PART OF ΔF FOR HOMOGENEOUS ORDER PARAMETERS

Assuming that the orientational order parameters are homogeneous [see Eq. (2.52)], the expression (2.45) for ΔF^{LR} can be further simplified. Specifically, the two integrations normal to the walls can be rewritten as

$$\int_{z_{\min}}^{z_{\max}} dz_1 \int_{z_{\min}}^{z_{\max}} dz_2 g_{\mathrm{LR}}(z_{12})$$
$$= \frac{1}{2}\sqrt{\frac{5}{4\pi}}\left(\int_{z_{\min}}^{z_{\min}+\tilde{\sigma}_T} dz_1 \int_{z_{\min}}^{z_1+\tilde{\sigma}_T} dz_2 (z_{12}^2 - \tilde{\sigma}_T^2)/\tilde{\sigma}_T^3 \right.$$
$$+ \int_{z_{\min}+\tilde{\sigma}_T}^{z_{\max}-\tilde{\sigma}_T} dz_1 \int_{z_1-\tilde{\sigma}_T}^{z_1+\tilde{\sigma}_T} (z_{12}^2 - \tilde{\sigma}_T^2)/\tilde{\sigma}_T^3$$
$$\left. + \int_{z_{\max}-\tilde{\sigma}_T}^{z_{\max}} dz_1 \int_{z_1-\tilde{\sigma}_T}^{z_{\max}} (z_{12}^2 - \tilde{\sigma}_T^2)/\tilde{\sigma}_T^3 \right)$$
$$= \frac{1}{2}\sqrt{\frac{5}{4\pi}}\left(-\frac{4}{3}L_z + \frac{11}{6}\tilde{\sigma}_T \right), \tag{A1}$$

where we have used Eqs. (2.44) and (2.16). Inserting Eq. (A1) into Eq. (2.45) and setting $\alpha_{1m}(z)=\alpha_{1m}$ we obtain

$$\frac{\Delta F^{\mathrm{LR}}}{\mathcal{V}} = -\frac{\rho^2}{2} 2\pi\gamma\mu^2 \frac{1}{2}\sqrt{\frac{5}{4\pi}} \frac{1}{(L_z - \tilde{\sigma}_T)} \left(-\frac{4L_z}{3} + \frac{11\tilde{\sigma}_T}{6} \right)$$
$$\times [C(112,000)\alpha_{10}^2 - 2C(112,1\underline{1}0)|\alpha_{11}|^2]. \tag{A2}$$

Finally, using the relations $C(112,000)=2\sqrt{1/6}$, $C(112,1\underline{1}0)=\sqrt{1/6}$, and $\gamma=8\pi\sqrt{2\pi/15}$, one arrives at Eq. (2.53).

APPENDIX B: DENSITY FUNCTIONAL OF THE BULK SYSTEM

Using the expansion (2.55) and evaluating the bulk free energy within the (truncated) MMF approximations described in Sec. II B 2, the grand canonical functional becomes

$$\frac{\Omega^b[\rho]}{\mathcal{V}} = k_B T\rho[\ln(\rho\Lambda^3) - 1] - \mu_{\mathrm{chem}}\rho$$
$$+ k_B T\rho \int d\omega \alpha(\cos\theta) \ln 4\pi\alpha(\cos\theta)$$
$$+ k_B T\rho \frac{4\eta_T - 3\eta_T^2}{(1-\eta_T)^2} + \frac{\Delta F^b}{\mathcal{V}}, \tag{B1}$$

where the contribution of the LJ- and dipolar interactions is given by

$$\frac{\Delta F^b}{\mathcal{V}} = -\frac{\rho^2 2\pi}{\beta} \int_{\tilde{\sigma}_T}^{\infty} dr_{12} r_{12}^2 \{\exp[-\beta u^{\mathrm{LJ}}(r_{12})] - 1\}$$
$$- \rho^2 \beta\mu^4 \frac{16\pi^{5/2}}{15} \int_{\tilde{\sigma}_T}^{\infty} dr_{12} r_{12}^4 \exp[-\beta u^{\mathrm{LJ}}(r_{12})]$$
$$\times \left(\frac{5}{8\pi^{3/2}} + \frac{2\sqrt{\pi}}{25}(\alpha_2^b)^2 \right) + \frac{\Delta F^{b,\mathrm{LR}}}{\mathcal{V}}. \tag{B2}$$

The last contribution in Eq. (B2) stems from the long-ranged part of the Mayer function [see Eq. (2.22)]. Evaluating this contribution in the absence of depolarizing fields (i.e., for a needlelike volume [31] with its long axis along the z direction), one obtains

$$\frac{\Delta F^{b,\mathrm{LR}}}{\mathcal{V}} = -\rho^2\mu^2 \frac{32\pi^3}{27}(\alpha_1^b)^2 = -\rho^2\mu^2 \frac{2\pi}{3} P_z^2. \tag{B3}$$

In obtaining the second line of Eq. (B3) we have used the relation $\alpha_1^b = (3/4\pi)P_z$, with P_z being the (homogeneous) polarization in the z direction. The resulting expression for $\Delta F^{b,\mathrm{LR}}$ corresponds to the *energy* of a macroscopic, homogeneously polarized sample in the absence of depolarizing fields.

[1] L. D. Gelb, K. E. Gubbins, R. Radhakrishnan, and M. Sliwinska-Bartkowiak, Rep. Prog. Phys. **62**, 1573 (1999).
[2] H. Nakanishi and M. E. Fisher, J. Chem. Phys. **78**, 3279 (1983).
[3] R. Evans, J. Phys.: Condens. Matter **2**, 8989 (1990).
[4] M. Schoen and D. J. Diestler, J. Chem. Phys. **109**, 5596 (1998).
[5] R. Evans, in *New Approaches to Problems in Liquid State Theory*, edited by C. Caccamo, J.-P. Hansen, and G. Stell, Vol. 529 of NATO ASI Series C: Mathematical and Physical Sciences (Kluwer Academic Publishers, Dordrecht, 1999).
[6] C. Alba-Simionesco, B. Coasne, G. Dosseh, G. Dudziak, K. E. Gubbins, R. Radnakrishnan, and M. Sliwinska-Bartkowiak, J. Phys.: Condens. Matter **18**, R15 (2006).
[7] A. Poniewierski and T. J. Sluckin, Liq. Cryst. **2**, 281 (1987).
[8] A. Poniewierski and T. J. Sluckin, Mol. Cryst. Liq. Cryst. **179**, 349 (1990).
[9] M. Dijkstra, R. van Roij, and R. Evans, Phys. Rev. E **63**, 051703 (2001).
[10] E. Gwozdz, K. Pasterny, and A. Brodka, Chem. Phys. Lett. **329**, 106 (2000).
[11] I. Rodriguez-Ponce, J. M. Romero-Enrique, and L. F. Rull, Phys. Rev. E **64**, 051704 (2001).
[12] S. H. L. Klapp and M. Schoen, J. Chem. Phys. **117**, 8050 (2002).
[13] S. H. L. Klapp and M. Schoen, J. Mol. Liq. **109**, 55 (2004).
[14] M. E. van Leeuwen, Fluid Phase Equilib. **99**, 1 (1994).
[15] M. E. van Leeuwen, B. Smit, and E. Hendriks, Mol. Phys. **78**, 271 (1993).
[16] M. J. Stevens and G. S. Grest, Phys. Rev. E **51**, 5976 (1995).
[17] G. T. Gao and X. C. Zeng, Phys. Rev. E **61**, R2188 (2000).
[18] M. E. van Leeuwen and B. Smit, Phys. Rev. Lett. **71**, 3991 (1993).
[19] P. J. Camp, J. C. Shelley, and G. N. Patey, Phys. Rev. Lett. **84**, 115 (2000).
[20] M. Schoen, in *Computational Methods in Surface and Colloid Science*, edited by M. Borowko (Marcel Dekker, New York, 2000), p. 1.
[21] S. H. Lee, J. C. Rasaiah, and J. B. Hubbard, J. Chem. Phys. **85**, 5232 (1986).
[22] S. H. Lee, J. C. Rasaiah, and J. B. Hubbard, J. Chem. Phys. **86**, 2383 (1987).

[23] C. N. Patra and S. K. Gosh, J. Chem. Phys. **106**, 2752 (1997).
[24] S. Senapati and A. Chandra, J. Chem. Phys. **111**, 1223 (1999).
[25] G. T. Gao, X. C. Zeng, and W. Wang, J. Chem. Phys. **106**, 3311 (1997).
[26] W. Jin and W. Wang, J. Chem. Phys. **114**, 10163 (2001).
[27] M. Sliwinska-Bartkowiak, G. Dudziak, R. Sikorski, R. Gras, K. E. Gubbins, and R. Radhakrishnan, Phys. Chem. Chem. Phys. **3**, 1179 (2001).
[28] P. I. Teixeira and M. M. Telo da Gama, J. Phys.: Condens. Matter **3**, 111 (1991).
[29] P. Frodl and S. Dietrich, Phys. Rev. A **45**, 7330 (1992).
[30] J. M. Tavares, M. M. Telo da Gama, P. I. C. Teixeira, J.-J. Weis, and M. J. P. Nijmeijer, Phys. Rev. E **52**, 1915 (1995).
[31] B. Groh and S. Dietrich, Phys. Rev. E **50**, 3814 (1994).
[32] B. Groh and S. Dietrich, Phys. Rev. Lett. **72**, 2422 (1994).
[33] G. M. Range and S. H. L. Klapp, Phys. Rev. E **69**, 041201 (2004).
[34] J. Israelachvili, *Intermolecular and Surface Forces*, 2nd ed. (Academic, London, 1992).
[35] F. Mugele and M. Salmeron, Phys. Rev. Lett. **84**, 5796 (2000).
[36] J. A. Barker and D. Henderson, J. Chem. Phys. **47**, 4714 (1967).
[37] C. F. Boettcher, *Theory of Electric Polarization*, 2nd ed. (Elsevier, New York, 1973).
[38] B. Groh and S. Dietrich, Phys. Rev. Lett. **79**, 749 (1997).
[39] B. Groh and S. Dietrich, Phys. Rev. E **57**, 4535 (1998).
[40] B. Groh and S. Dietrich, Phys. Rev. E **53**, 2509 (1996).
[41] C. G. Gray and K. E. Gubbins, *Theory of Molecular Fluids* (Oxford University, London, 1984), Vol. 1.
[42] N. F. Carnahan and K. E. Starling, J. Chem. Phys. **51**, 635 (1969).
[43] Note that our definition of the rotational invariants differs from that given in Ref. [41] by a prefactor $\sqrt{4\pi/(2l_1+1)(2l_2+1)}$.
[44] S. H. L. Klapp, Mol. Simul. **32**, 609 (2006).
[45] A. Schreiber, H. Bock, M. Schoen, and G. Findenegg, Mol. Phys. **100**, 2097 (2002).
[46] J. J. Weis, D. Levesque, and G. J. Zarragoicoechea, Phys. Rev. Lett. **69**, 913 (1992).
[47] E. Gedat, A. Schreiber, J. Albrecht, T. Emmler, I. Shenderovich, G. H. Findenegg, H. H. Limbach, and G. Buntkowsky, J. Phys. Chem. B **106**, 1977 (2002).
[48] V. Froltsov and S. H. L. Klapp, J. Chem. Phys. **124**, 134701 (2006).
[49] Y. Rosenfeld, Phys. Rev. Lett. **63**, 980 (1989).